iScience

CellPress
OPEN ACCESS

Article

Spatiotemporal dynamics exhibited by horizontal basal cells reveal a pro-neurogenic pathway during injury-induced olfactory epithelium regeneration

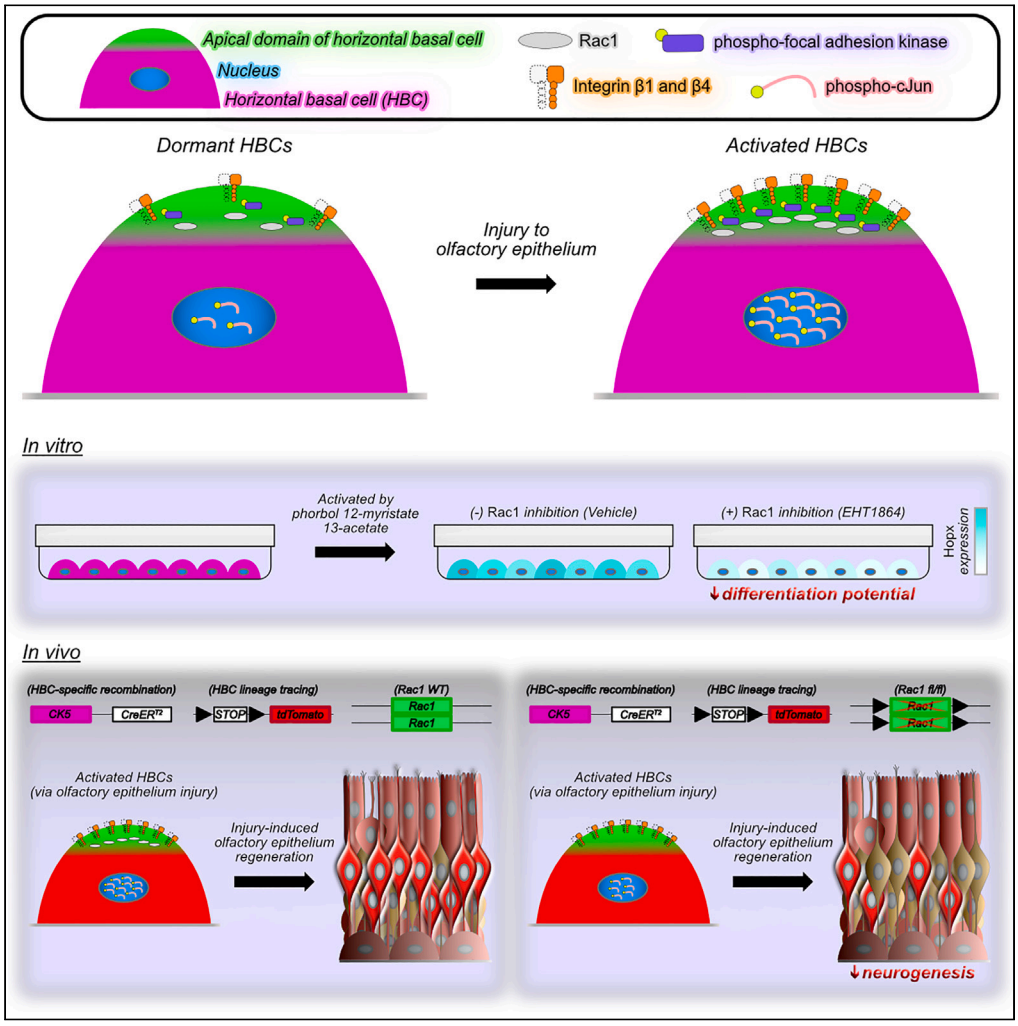

Jonathan D. Louie, Camila M. Barrios-Camacho, Benjamin H. Bromberg, Constantin A. Hintschich, James E. Schwob

jim.schwob@tufts.edu

Highlights

Activated HBCs *in vivo* increase Rac1 within their apical domain following OE injury

Rac1-mediated signaling within activated HBCs *in vitro* is impaired by Rac1 inhibition

Differentiation potential of activated HBCs *in vitro* is attenuated by Rac1 inhibition

In vivo HBC neurogenesis following OE injury is impaired by HBC-specific *Rac1* cKO

Louie et al., iScience 27, 109600 May 17, 2024
https://doi.org/10.1016/j.isci.2024.109600

iScience

CellPress
OPEN ACCESS

Article

Spatiotemporal dynamics exhibited by horizontal basal cells reveal a pro-neurogenic pathway during injury-induced olfactory epithelium regeneration

Jonathan D. Louie,[1,2,3] Camila M. Barrios-Camacho,[2,3] Benjamin H. Bromberg,[3] Constantin A. Hintschich,[3,4,5] and James E. Schwob[3,6,*]

SUMMARY

Horizontal basal cells (HBCs) mediate olfactory epithelium (OE) regeneration following severe tissue injury. The dynamism of the post-injury environment is well illustrated by *in silico* modeling of RNA sequencing data that demonstrate an evolving HBC transcriptome. Unfortunately, spatiotemporally dynamic processes occurring within HBCs *in situ* remain poorly understood. Here, we show that HBCs at 24 h post-OE injury spatially redistribute a constellation of proteins, which, in turn, helped to nominate Rac1 as a regulator of HBC differentiation during OE regeneration. Using our primary culture model to activate HBCs pharmacologically, we demonstrate that concurrent Rac1 inhibition attenuates HBC differentiation potential. This *in vitro* functional impairment manifested *in vivo* as decreased HBC differentiation into olfactory sensory neurons following HBC-specific *Rac1* conditional knockout. Taken together, our data potentiate the design of hyposmia-alleviating therapies and highlight aspects of *in situ* HBC spatiotemporal dynamics that deserve further investigation.

INTRODUCTION

Exposed to the external environment, the olfactory epithelium (OE) is a specialized neuroepithelium composed of sensory neurons and non-neuronal cell types that collectively facilitate transduction of volatile odorants. Critical to OE homeostasis, a population of reserve resident stem cells called horizontal basal cells (HBCs) reside atop the basal lamina. While typically dormant, HBCs activate and contribute to OE regeneration following severe tissue injury.[1] Various mechanisms promote HBC-mediated OE repair, including those derived non-cell autonomously from the surrounding tissue environment. For example, targeted ablation of glial-like sustentacular (Sus) cells whose cell bodies form the OE-nasal cavity interface and extend processes basally that run adjacent to HBCs[2] leads to HBC differentiation.[3] This process following Sus cell destruction has been postulated to result from decreased cell-cell interactions between the Sus cell-expressed Notch ligand, Jagged1, and Notch1 receptor expressed by HBCs.[3] Additionally, Sus cell destruction is thought to cause a localized reduction of retinoic acid, a cytokine synthesized by Sus cells that specifies HBC dormancy.[4] Severe injury also elicits an inflammatory response that appears to regulate HBCs.[5] Diminution of this response or impairing the ability of HBCs to respond to inflammatory cytokines negatively impacts HBC proliferation and subsequent OE regeneration.[5] Moreover, discovery that HBC-specific ablation of cilia compromises OE regeneration further emphasizes the importance of extrinsic, environmental cues[6] to HBC-mediated tissue repair.

Complementing these non-cell autonomous processes, ΔNp63 (p63) is a transcription factor that positively regulates HBC dormancy.[7] Therefore, p63 downregulation is both necessary and sufficient to activate HBCs so that these resident stem cells can appropriately participate in OE regeneration.[8] The critical relationship between p63 and HBC activation is underscored by HBC-specific *p63* conditional knockout (cKO) that results in aberrant HBC differentiation within uninjured OE,[7,8] and, conversely, p63 overexpression that attenuates basal cell differentiation following OE injury.[8] Additionally, RNA sequencing technology has been a boon for computationally modeling HBCs to visualize their highly dynamic genomic landscape *in silico* following p63 downregulation.[9,10] To date, however, little is known about the spatiotemporal dynamics exhibited by HBCs *in situ* soon after injury, and whether such dynamic processes involve a molecular component central to HBCs and their ability to contribute to OE regeneration.

To address this gap in knowledge, subcellular protein distribution within HBCs was assessed by dividing these stem cells into multiple intracellular domains. Comparing HBCs within uninjured and acutely injured OE revealed a constellation of differentially expressed proteins

[1]Medical Scientist Training Program, Tufts University School of Medicine, Boston, MA 02111, USA
[2]Neuroscience Graduate Program, Tufts University Graduate School of Biomedical Sciences, Boston, MA 02111, USA
[3]Department of Developmental, Molecular & Chemical Biology, Tufts University Graduate School of Biomedical Sciences, Boston, MA 02111, USA
[4]Department of Otorhinolaryngology, University Hospital Regensburg, Franz-Josef-Strauß-Allee 11, 93053 Regensburg, Germany
[5]Department of Otolaryngology, Massachusetts Eye and Ear Infirmary, Harvard Medical School, Boston, MA 02114, USA
[6]Lead contact
*Correspondence: jim.schwob@tufts.edu
https://doi.org/10.1016/j.isci.2024.109600

suggesting that Rac1 may influence HBCs as they mediate OE regeneration. Using our previously described primary HBC culture models[11,12] to inform our *in vivo* investigation, the data in sum demonstrate that Rac1 positively regulates HBC neurogenesis. Furthermore, our work here establishes an *in vitro* model's utility for elucidating mechanisms that govern HBC biology and provides the rationale for new avenues of exploration that may further enhance our understanding of HBCs.

RESULTS

HBCs at 24 h post-injury (24 hpi) increase their apical expression of integrin β1 (Itgb1) and integrin β4 (Itgb4)

As p63 positively regulates HBC dormancy within the OE, its decline is sufficient to shift HBCs away from dormancy and serve as a marker of HBC activation.[7,8] Relative to those within uninjured OE, cytokeratin 5$^+$ (CK5$^+$) HBCs in wild-type (WT) mice significantly downregulate p63 expression 24 h after intra-peritoneal injection with methimazole (MTZ) (Figures 1A–1E), an olfactotoxic agent known to induce severe OE injury that results in HBC-mediated regeneration of the tissue.[1,13] Given that p63 can positively regulate expression of Itgb1 and Itgb4,[14] it was therefore surprising that HBCs at 24 hpi did not decrease total Itgb1 (Figures S1A, S1B, S1E, S1F, and S1I) nor total Itgb4 relative to expression within uninjured OE (Figures S1K, S1L, S1O, S1P, and S1S) as defined by their respective fluorescence intensities within CK5$^+$ HBCs. Because activated HBCs have been shown to undergo morphological changes suggestive of diminished contact with the basal lamina,[8] it was also surprising that HBCs at 24 hpi do not decrease basal Itgb1 (Figures S1C, S1D, S1G, S1H, and S1J) nor basal Itgb4 (Figures S1M, S1N, S1Q, S1R, and S1T) relative to their counterparts within uninjured OE as defined by integrin fluorescence intensity within areas exclusively labeled by CK5 and the basal lamina constituent, Laminin. Notably, however, HBCs at 24 hpi increase apical domain expression of Itgb1 and Itgb4 by 91.2% (Figures 1F–1N) and 131.9% (Figures 1O–1W), respectively, relative to those within uninjured OE. For this analysis, the apical domain was defined as areas labeled by both CK5 and Ezrin (Figures 1H, 1I, 1L, 1M, 1Q, 1R, 1U, and 1V), the latter of which is a protein that regulates apical domain integrity by linking other apically localized proteins to the cytoskeleton.[15] As such, these data demonstrate that, at 24 hpi, HBCs spatially modulate intracellular protein expression in part by enhancing apical expression of Itgb1 and Itgb4.

HBCs at 24 hpi spatiotemporally synchronize intracellular focal adhesion components that suggest enhancement of Rac1-mediated signaling pathway activity

The cytoplasmic tails of both Itgb1 and Itgb4 can activate Rac1,[16–18] a member of a family of small Rho GTPases[19,20] that can mediate various stem cell functions.[21–24] Concomitant with increased apical localization of Itgb1 and Itgb4 (Figures 1F–1W), HBCs at 24 hpi notably increase apical Rac1 by 81.6% relative to HBCs in uninjured OE (Figures 2A–2G). Furthermore, focal adhesion kinase phosphorylated at tyrosine 925 (pFAKY925), a critical intermediary that facilitates integrin-mediated Rac1 activation,[25] is similarly increased by 91.7% in the apical domain of HBCs at 24 hpi when compared to the apical domain of HBCs prior to OE injury (Figures 2H–2N). Interestingly, the spatiotemporal synchronicity that HBCs demonstrate via enhanced apical localization of Itgb1 and Itgb4, pFAKY925, and Rac1 coincides with a greater than 8-fold increase in HBC expression of pcJun (Figures 2O–2U), a transcription factor subunit that can participate in regulating proliferation and tissue morphogenesis.[26–28] As pcJun lies downstream of Rac1 activation,[29] these data in sum suggest that HBCs at 24 hpi enhance Rac1-mediated signaling pathways.

HBC expression of Rac1 within the regenerating OE progressively wanes

At 2 and 3 days post-injury (dpi), distinct layers of cells begin to comprise the regenerating OE. Within these layers reside p63$^+$ HBCs and p63$^-$ non-HBCs[30] (Figure S2). Using the *CK5* promoter to drive expression of tamoxifen-inducible *Cre recombinase* and lineage trace tdTomato$^+$ (tdTom$^+$) HBCs and their progeny (*K5CreER^{T2}*; *Rosa26R(tdTomato)*), p63$^-$/tdTom$^+$ non-HBCs within these bi-genic mice at 2 dpi express 25.5% more Rac1 relative to p63$^+$/tdTom$^+$ HBCs (Figures S2A–S2E). At 3 dpi, Rac1 becomes increasingly enriched to p63$^-$/tdTom$^+$ non-HBCs (32.6%) (Figures S2F–S2J). These data demonstrate that Rac1 segregates away from HBCs as OE regeneration proceeds, thereby further suggesting that HBCs may only acutely utilize Rac1-mediated signaling after OE injury (Figures 1 and 2).

Primary HBCs activated *in vitro* demonstrate molecular sensitivity to Rac1 inhibition

To begin interrogating the potential relationship between HBC activation and Rac1 function, we leveraged our HBC culture system that enables transcriptional recapitulation of *in vivo* HBCs[11] to treat primary HBCs with phorbol 12-myristate 13-acetate (PMA), a compound used to activate other stem cells *in vitro*.[31,32] Importantly, *in vitro* rat HBCs treated for 12 h with 50 nM PMA emulate a myriad of transcriptomic patterns exhibited by *in vivo* HBCs through 24 hpi[12] when they spatiotemporally synchronize a constellation of molecular components suggestive of Rac1-mediated signaling activity (Figures 1 and 2). Expectedly, 50 nM PMA treatment triggers HBC activation as evidenced by decreased p63 abundance when compared to vehicle-treated HBCs (Figures 3A and 3B). Mirroring the molecular characteristics exhibited by *in vivo* HBCs at 24 hpi (Figures 1A–1E and 2O–2U), p63 downregulation *in vitro* occurs concomitant with increased pcJun abundance (Figures 3A and 3D). To determine whether this increase in pcJun was a result of Rac1 activation, PMA-induced HBC activation was coupled with 50 μM EHT1864, an inhibitor of Rac1 activity.[33] Indeed, PMA and EHT1864 treatment together attenuated pcJun abundance by 36.8% relative to PMA alone (Figures 3A and 3D). As Rac1 activation facilitates pcJun expression via upstream phosphorylation of cJun N-terminal kinase (JNK),[34,35] the same treatment paradigm similarly decreased pJNK abundance by 37.1% relative to PMA alone (Figure S3), thus underscoring the involvement of Rac1-mediated signaling. Importantly, these effects were not due to any significant change in total Rac1 abundance (Figures 3A and 3C). Notably, the decrease in p63 abundance with concurrent PMA and EHT1864 treatment was not significantly different

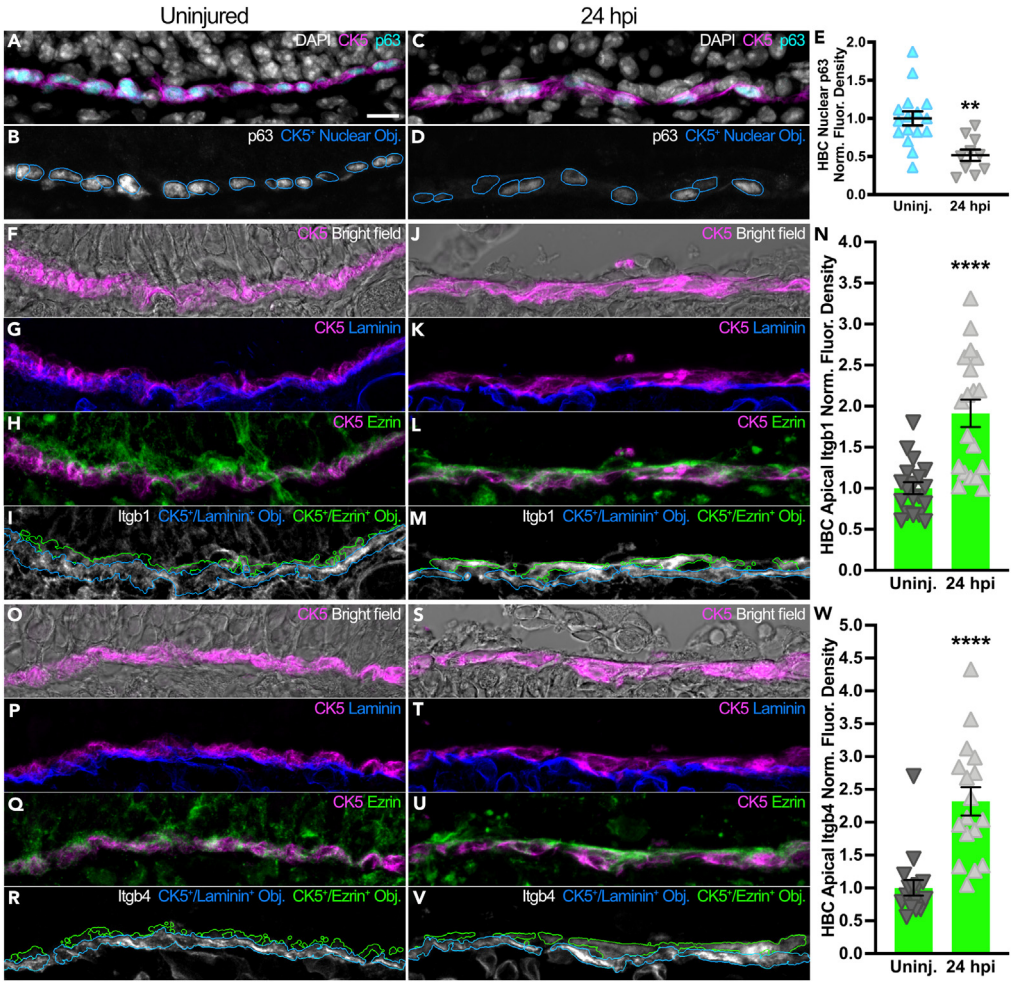

Figure 1. HBCs at 24 hpi increase apical expression of Itgb1 and Itgb4

(A–D) Representative immunofluorescence images demonstrating that relative to HBCs within uninjured (uninj.) OE (A, B), HBCs at 24 hpi are activated as they demonstrate p63 downregulation (C, D).

(E) Quantification of nuclear p63 normalized (norm.) fluorescence (fluor.) density within $CK5^+$ HBCs; each triangle represents a $CK5^+$ Nuclear Object (Obj.) (blue outlines in B and D) used to quantify the encompassed p63 fluorescence.

(F–M) Representative immunofluorescence images demonstrating that HBCs at 24 hpi (J–M) increase apical Itgb1 (within green outlines, I and M) relative to HBCs within uninj. OE (F–I).

(N) Quantification of Itgb1 norm. fluor. density within HBC apical domains; each triangle denotes an analyzed region as represented in (I) and (M) (n = 19 regions across 3 mice).

(O–V) Representative immunofluorescence images demonstrating that HBCs at 24 hpi (S–V) increase apical Itgb4 (within green outlines, R and V) relative to HBCs within uninj. OE (O–R).

(W) Quantification of Itgb4 norm. fluor. density within HBC apical domains; each triangle denotes an analyzed region as represented in (R) and (V) (n = 17 regions across 3 mice). Unpaired t test (E, J), Mann-Whitney test (O). Uninj. used as baseline, error bars indicate mean ± SEM, $^{**}p < 0.01$, $^{****}p < 0.0001$ (E, N, W). Scale bar equals 10 μm (A).

relative to PMA alone (Figure 3B). Collectively, these data demonstrate that primary HBCs enhance Rac1-mediated signaling following their activation *in vitro*, which in turn suggest that HBCs do so to regulate a currently undefined process independent of their activation.

Rac1-mediated signaling influences primary HBC differentiation potential

As activated HBCs in culture exhibited molecular sensitivity to concurrent Rac1 inhibition (Figures 3 and S3), we examined how inhibiting Rac1 in PMA-activated *in vitro* rat HBCs might alter their function. Notably, *in vivo* HBCs become increasingly proliferative[7] and upregulate *Hopx*, an early marker of HBC differentiation,[10] shortly after their activation. Relative to HBCs treated with vehicle, PMA treatment alone more than doubled overall Hopx expression (Figures 4A, 4B, and 4E). When concurrently treated with PMA and EHT1864, HBC expression of Hopx was diminished by 43.8% relative to PMA alone (Figures 4B, 4C, and 4E). Surprisingly, *in vitro* HBCs attenuated Ki67 expression by nearly 25%

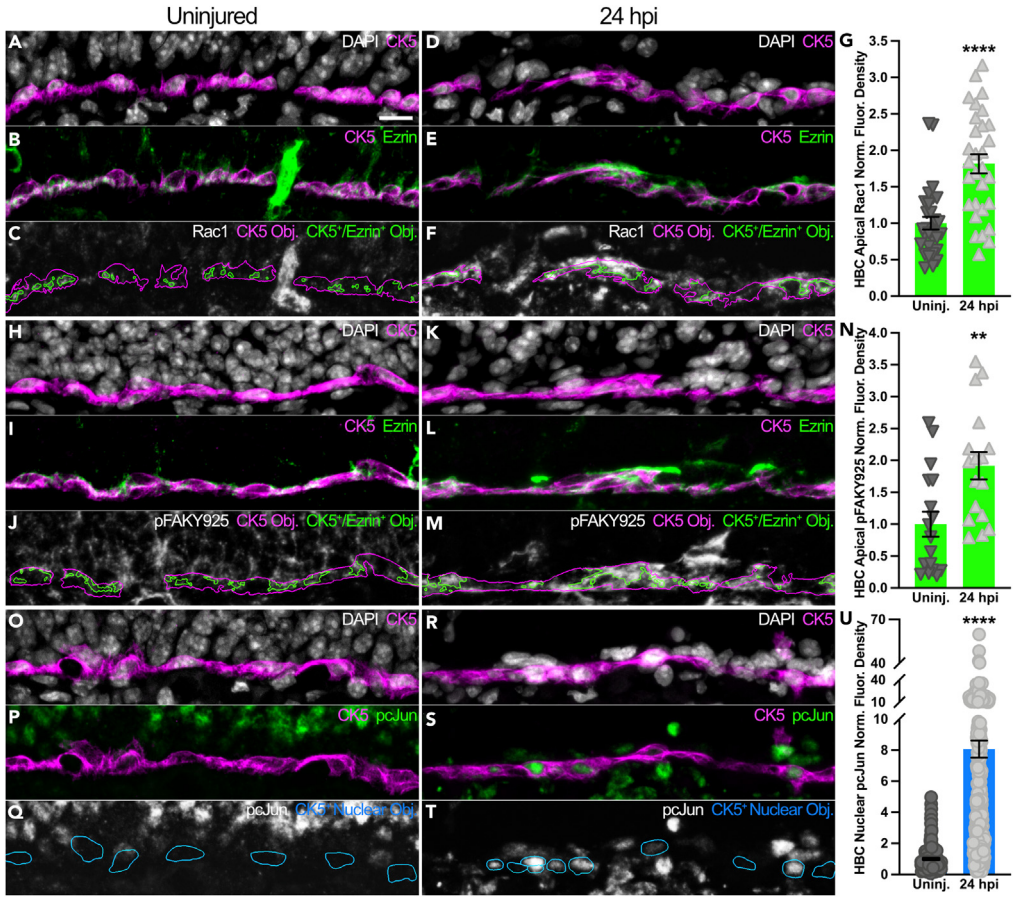

Figure 2. HBCs at 24 hpi spatiotemporally synchronize Rac1 with another intracellular focal adhesion component and a downstream effector of Rac1-mediated signaling

(A–F) Representative immunofluorescence images demonstrating that HBCs at 24 hpi (D–F) upregulate apical Rac1 (within green outlines, C and F) relative to HBCs within uninj. OE (A–C).

(G) Quantification of Rac1 norm. fluor. density within HBC apical domains; each triangle denotes an analyzed region as represented in (C) and (F) (n = 30 regions across 3 mice).

(H–M) Representative immunofluorescence images demonstrating that HBCs at 24 hpi (K–M) upregulate apical pFAKY925 (within green outlines, J and M) relative to HBCs within uninj. OE (H–J).

(N) Quantification of pFAKY925 norm. fluor. density within HBC apical domains; each triangle denotes an analyzed region as represented in (J) and (M) (n = 17 regions across 3 mice).

(O–T) Representative immunofluorescence images demonstrating that HBCs at 24 hpi (R–T) upregulate nuclear pcJun (within blue outlines, Q and T) relative to HBCs within uninj. OE (O–Q).

(U) Quantification of pcJun norm. fluor. density within HBC nuclei; each circle denotes a $CK5^+$ Nuclear Obj. as represented in (Q) and (T) (n = 3 mice, 234 uninj. HBCs and 258 24 hpi HBCs). Uninj. used as baseline; error bars indicate mean ± SEM, Mann-Whitney test, $^{**}p < 0.01$, $^{****}p < 0.0001$ (G, N, U). Scale bar equals 10 μm (A).

following treatment with PMA in comparison to vehicle treatment (Figures 4F, 4G, and 4J). Treatment with both small molecules also resulted in a small, but statistically significant, decrease in overall Ki67 expression relative to PMA treatment alone (~2.2%) (Figures 4G, 4H, and 4J). Together, these data demonstrate that inhibition of Rac1-mediated signaling functionally disrupts HBCs following their *in vitro* activation by PMA.

In vivo HBCs at 24 hpi engage in Rac1-mediated signaling

Given that primary HBCs *in vitro* subjected to concurrent small molecule-mediated activation and Rac1 inhibition demonstrated diminished pcJun abundances (Figures 3A and 3D), we interrogated whether *in vivo* HBCs engage in Rac1-mediated signaling activity. To do so, we utilized tri-genic mice expressing tamoxifen-inducible *Cre recombinase* driven by the *CK5* promoter to simultaneously conditionally knock out *Rac1* (Figures S4 and S5) in an HBC-specific manner and identify HBCs and their progeny via a tdTom reporter (*K5CreER^{T2}*; *Rac1$^{fl/fl}$*; *Rosa26R(tdTomato)*, hereafter referred to as *Rac1* fl/fl). These *Rac1* fl/fl mice were compared to *Rac1* WT mice in which both *Rac1* alleles are WT but otherwise similarly harbor *CK5*-driven *Cre recombinase* and the conditional tdTom reporter to identify HBCs and their derivatives.

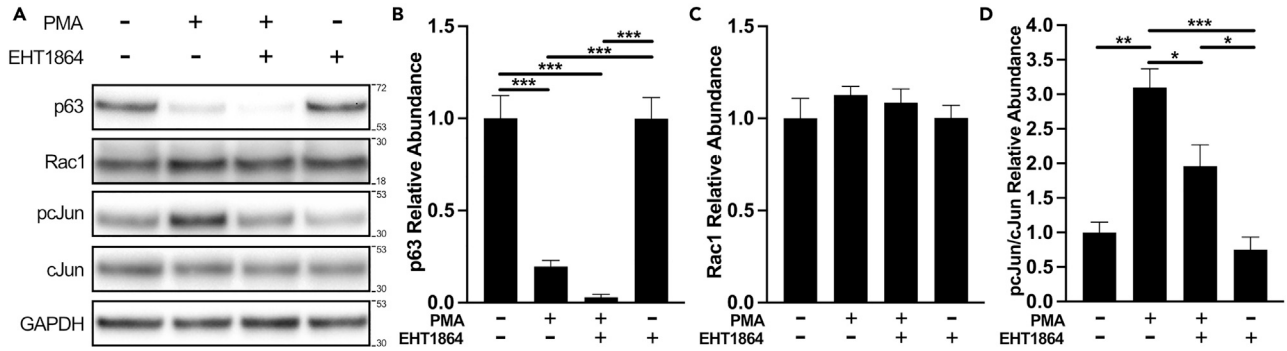

Figure 3. Primary HBCs activated *in vitro* enhance Rac1-mediated signaling

(A) Representative western blots depicting p63, Rac1, pcJun, total cJun, and GAPDH abundances in cultures of vehicle-treated (PMA-/EHT1864-), activated (PMA+/EHT1864-), activated and Rac1 inhibited (PMA+/EHT1864-), and Rac1 inhibited (PMA-/EHT1864+) HBCs.

(B–D) Quantification of densitometric measurements for p63 (B), Rac1 (C), and normalized pcJun per normalized total cJun (D) abundances (n = 3 independent trials), vehicle-treated used as baseline, error bars indicate mean +SEM, one-way ANOVA with *post hoc* Tukey's multiple comparisons test, *<0.05, **p < 0.01, ***p < 0.001.

Following MTZ-induced OE injury, HBCs within *Rac1* fl/fl OE at 24 hpi did not demonstrate a significant difference in nuclear p63 relative to their *Rac1* WT counterparts (Figures 5A–5C, 5F–5H, and 5K). HBC-specific *Rac1* cKO, however, decreased HBC nuclear pcJun by 44.5% (Figures 5D, 5E, 5I, 5J, and 5L). Taken together, the molecular consequences of *in vivo* Rac1 perturbation recapitulate those observed *in vitro* (Figures 3B and 3D) and demonstrate that Rac1 mediates signaling within *in vivo* HBCs following OE injury.

Rac1 regulates the neurogenic potential of *in vivo* HBCs during OE regeneration

As *in vivo* HBCs utilize Rac1-mediated signaling pathways soon after HBC-mediated OE regeneration initiates, we examined the potential functional consequences of HBC-specific *Rac1* cKO. Although Rac1 has been shown to organize integrin expression,[36,37] Itgb1 (Figures S6A–S6M) and Itgb4 (Figures S6N–S6Z) localization to HBC intracellular domains was not affected within *Rac1* fl/fl OE. Due to an inability in our hands to immunolabel Hopx within OE tissue sections, we were unable to correlate *in vivo* the dramatic downregulation of Hopx demonstrated by *in vitro* HBCs following their concurrent activation and Rac1 inhibition (Figures 4B, 4C, and 4E). However, because Hopx labels HBCs determined to differentiate,[10] we interrogated the longer-term functional impact of Rac1 *in vivo* by assessing morphologically regenerated OE at 28 28 dpi in *Rac1* WT and *Rac1* fl/fl mice. *Hopx*-expressing HBCs primarily give rise to Sus cells and olfactory sensory neurons (OSNs),[10] with the former identifiable by CK8 and interleukin-33 (IL33) located apically within the regenerated tissue[10,38] while immature and mature OSNs are marked by PGP9.5.[30,39–42] Following OE injury, HBC differentiation into CK8$^+$/apical IL33$^+$/tdTom$^+$ Sus cells was unaffected (17.1 HBC-derived Sus cells per 100 μm *Rac1* fl/fl OE vs. 18.3 HBC-derived Sus cells per 100 μm *Rac1* WT OE) (Figures 6A–6K). Interestingly, however, HBC-specific *Rac1* cKO attenuated HBC differentiation into PGP9.5$^+$/tdTom$^+$ OSNs at 28 dpi by nearly half (14.6 HBC-derived OSNs per 100 μm *Rac1* fl/fl OE vs. 25.7 HBC-derived OSNs per 100 μm *Rac1* WT OE) (Figures 6L–6V). In sum, these data demonstrate that Rac1 positively regulates the magnitude of HBC-derived neurogenesis during OE regeneration.

DISCUSSION

While it has been known for more than a decade that HBCs can help repair the OE following tissue injury,[1] the transcriptional and environmental mechanisms that enable HBC-mediated OE regeneration have only relatively recently been explored.[5,6,8,30] However, it still remains unknown whether HBCs *in situ* exhibit processes that are spatiotemporally dynamic across subcellular domains soon after tissue injury and, if so, whether any of these early molecular players facilitates appropriate HBC contribution to OE reconstitution. We show here that HBCs reorganize Rac1 apically following OE injury. Subsequent to identifying this biological phenomenon, we interrogated these OE-resident stem cells in culture and *in vivo*. These investigations demonstrated for the first time that Rac1 regulates HBC differentiation potential *in vitro* and HBC neurogenesis during *in vivo* injury-induced OE regeneration.

The need to better understand HBC biology arises from the prevalence of olfactory deficits and their associated morbidities experienced by the aging population.[43,44] OE biopsies from dysosmic patients demonstrate aneuronal regions[42,45] that, despite the need for tissue repair, harbor persistently dormant HBCs.[46,47] As such, one strategy to ameliorate olfactory dysfunction and its burdens includes artificially activating this endogenous HBC population. An alternate approach capitalizes on the ability to harvest, expand, activate,[11] and re-introduce HBCs in an autologous manner. In either case, the mechanisms governing HBC differentiation need to be defined for therapeutic efficacy. Presently, inefficient HBC engraftment challenges the feasibility of cultured HBC transplantation,[11,12] and this hindrance recapitulates a rodent model of stem cell infusion into the auditory cochlea.[48] Their data in particular highlight the need to understand and regulate the differentiation of stem cells before transplantation, as evidenced by an inverse relationship between degree of cellular differentiation prior to infusion and cell survival following transplantation. Similar reasons may explain why HBCs, which upregulate the differentiation marker, Hopx, following PMA-mediated *in vitro* activation, exhibit low engraftment efficiency within injured OE. Notably, our *in vitro* data identify Rac1 as a positive

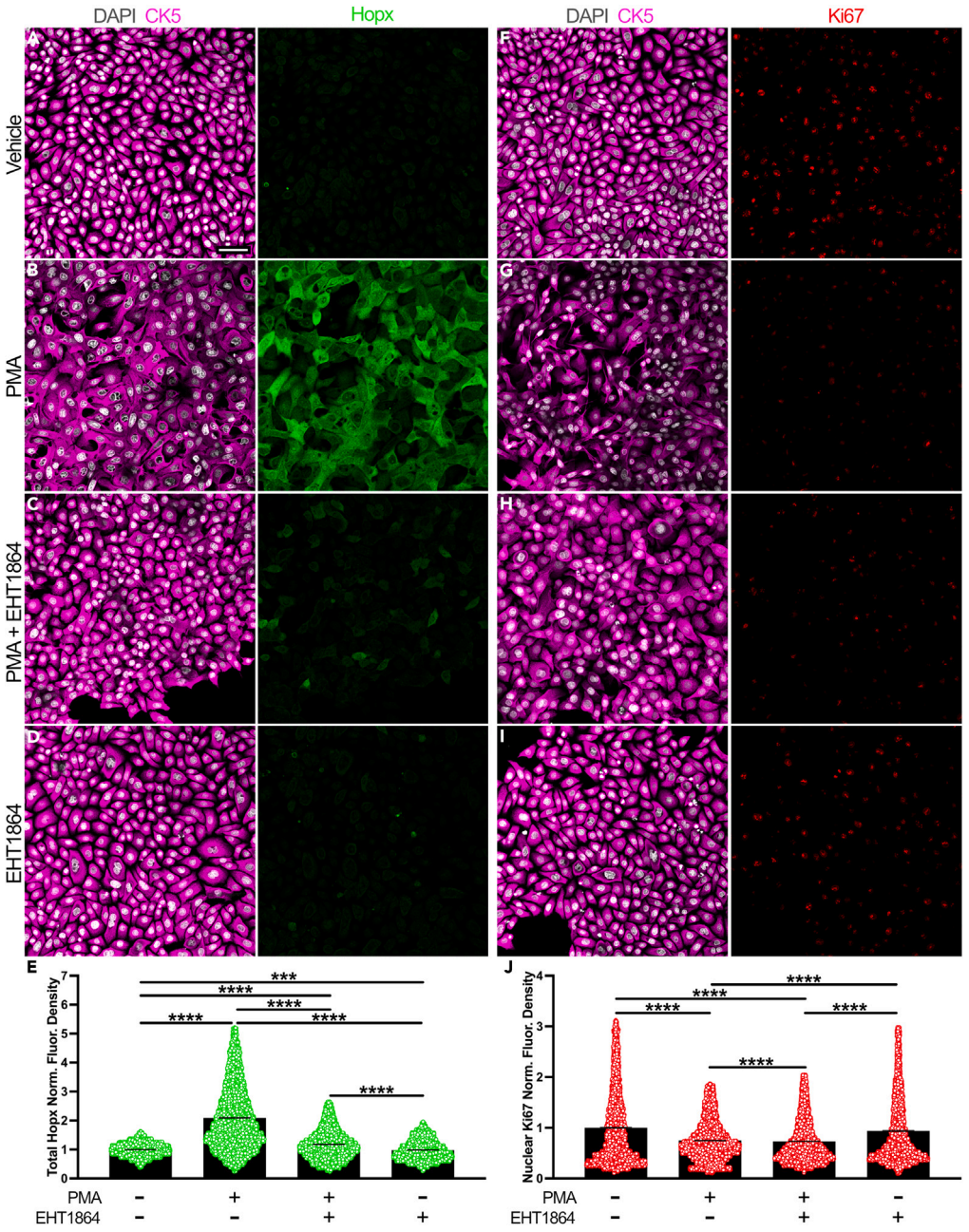

Figure 4. Rac1 potentiates primary HBC differentiation *in vitro*

(A–D) Representative immunofluorescence images of Hopx expression in cultures of vehicle-treated (A), activated (B), activated and Rac1 inhibited (C), and Rac1 inhibited (D) HBCs.

(E) Quantification of norm. total Hopx fluor. density for conditions represented in (A) (4,927 $CK5^+$ HBCs), (B) (8,065 $CK5^+$ HBCs), (C) (7,235 $CK5^+$ HBCs), and (D) (5,358 $CK5^+$ HBCs) (n = 4 independent trials), each circle represents an analyzed $CK5^+$ HBC.

(F–I) Representative immunofluorescence images of Ki67 expression in cultures of vehicle-treated (F), activated (G), activated and Rac1 inhibited (H), and Rac1 inhibited (I) HBCs.

(J) Quantification of norm. nuclear Ki67 fluor. density for conditions represented in (F) (4,716 $CK5^+$ HBCs), (G) (7,325 $CK5^+$ HBCs), (H) (7,297 $CK5^+$ HBCs), and (I) (5,228 $CK5^+$ HBCs) (n = 4 independent trials); each circle represents an analyzed $DAPI^+$ area within a $CK5^+$ HBC. Vehicle (PMA^-/$EHT1864^-$) used as baseline; error bars indicate mean ± SEM, Kruskal-Wallis test with *post hoc* Dunn's multiple comparisons test, ***p < 0.001, ****p < 0.0001 (E, J). Scale bar equals 50 μm (A).

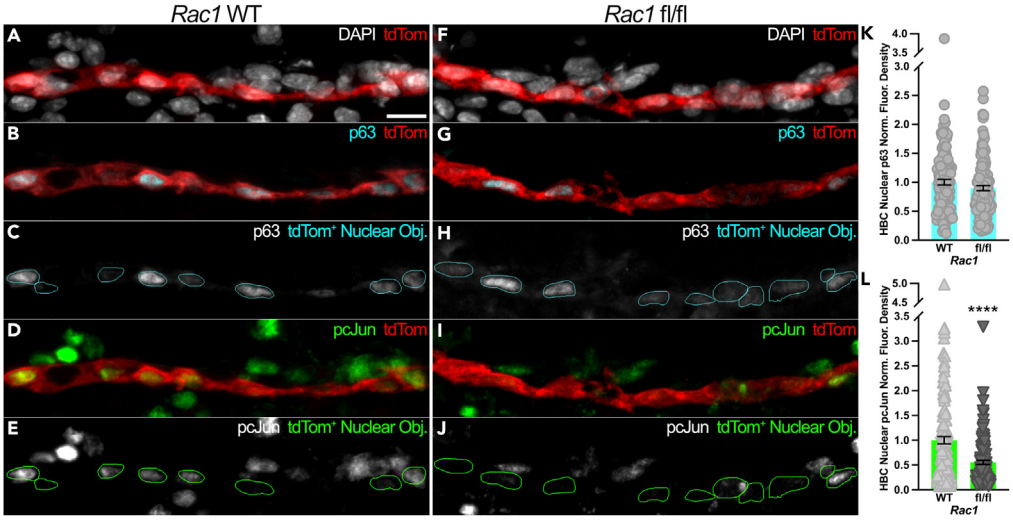

Figure 5. *In vivo* HBCs at 24 hpi demonstrate diminished Rac1-mediated signaling as a consequence of HBC-specific *Rac1* cKO

(A–L) Representative immunofluorescence images from *Rac1* WT (A–C) and *Rac1* fl/fl (F–H) OE demonstrate that HBC expression of nuclear p63 at 24 hpi (within cyan outlines, C and H) is not significantly affected by HBC-specific *Rac1* cKO (quantified in K, each circle denotes a tdTom$^+$ Nuclear Obj. as represented in C and H [n = 3 mice, 132 *Rac1* WT HBCs and 124 *Rac1* fl/fl HBCs]). Representative immunofluorescence images from *Rac1* WT (A, D, E) and *Rac1* fl/fl (F, I, J) OE demonstrate that nuclear pcJun at 24 hpi (within green outlines, E and J) is diminished by HBC-specific *Rac1* cKO (quantified in L, each triangle denotes a tdTom$^+$ Nuclear Obj. as represented in E and J [n = 3 mice, 132 *Rac1* WT HBCs and 124 *Rac1* fl/fl HBCs]). *Rac1* WT used as baseline, error bars indicate mean ± SEM, Mann-Whitney test, ****$p < 0.0001$ (K, L). Scale bar equals 10 μm (A).

regulator of HBC differentiation. Furthermore, concomitant PMA treatment with reversible inhibition of Rac1 attenuated Hopx without significantly affecting the decrease in p63 abundance that indicates HBC activation. Consequently, this present work offers a potential strategy to simultaneously improve HBC engraftment and maintain stem cell potency. Building from this framework, future investigations utilizing EHT1864 to optimize engraftment efficiency should remain mindful of the disparity between cellular and molecular processes. Although NIH 3T3 mouse fibroblasts attenuate lamellipodia formation after treatment with 5 μM EHT1864, BT-474 human breast cancer cells demonstrate an IC_{50} of 3.17 μM EHT1864 with respect to proliferation, and SH-SY5Y human neuroblastoma cells exhibit an IC_{50} of 5.44 μM in relation to Aβ plaque release, EHT1864 was required at much higher concentrations to inhibit Rac1 activity (50 μM, 50 μM, and >25 μM, respectively).[33,49,50] This process-dependent variability is also exemplified by cell death. While significant increases in apoptotic OCI-AML3 human acute myeloid leukemia and bladder smooth muscle cells were observed after treatment with 30 μM and 50 μM EHT1864, respectively,[51,52] rat HBCs in vehicle- and 50 μM EHT1864-treated cultures demonstrated similar morphological appearances (Figures 4A–4D, 4F, and 4I) and treated mouse platelets retained significant viability up to 200 μM EHT1864.[53]

The critical nature of reversible Rac1 inhibition for any potential HBC infusion therapy is underscored by HBC-specific *Rac1* cKO and its attenuation of *in vivo* HBC neurogenesis following OE injury. The consequences of *Rac1* cKO in the OE are consistent with Rac1's role in promoting hippocampal neurogenesis.[54–56] Although Rac1 has also been implicated in positively regulating glial differentiation,[57] *Rac1* cKO did not perturb HBC differentiation into Sus cells, which serve multiple glial-like functions within the OE such as regulating local metabolism, phagocytosis, and maintaining ion balance.[58–61] Furthermore, Sus cells are thought to specify HBC dormancy via direct cell-cell interactions[3] and contribute retinoic acid to the environmental milieu.[4] Given that these support cells serve functions critical to tissue homeostasis, it would be worthwhile to interrogate whether Rac1 within HBCs operates in parallel with other redundant, sufficient-but-not-necessary mechanisms to ensure HBC differentiation into Sus cells. Interestingly, Rac1 localization to Sus cells in addition to HBCs (Figure S5) may further underscore the former cell type's importance to overall OE integrity as this GTPase has been shown to promote tight junction formation.[62,63] It remains to be seen whether Sus cells, which immediately abut the nasal cavity that is in direct contact with the external environment, employ Rac1 as a mechanism to maintain OE barrier function. From an evolutionary perspective, the need to restore barrier function may explain why Sus cells can differentiate directly from HBCs without the need for intermediary progenitors,[10] which could represent possible failure points. Moreover, in light of unperturbed Sus cell differentiation following various HBC-specific manipulations[30] (Figures 6A–6K), the question of whether a subset of HBCs is already determined during OE development to become Sus cells upon their activation deserves examination.

As we demonstrated with Rac1 and HBC neurogenesis, 50 nM PMA can be used to activate HBCs *in vitro* as a starting point to elucidate mechanisms that govern HBC fate. In the present case, it is important to highlight that PMA treatment itself can lead to cJun phosphorylation via activation of protein kinase C,[64,65] which thus may explain the still significant but not overly dramatic decrease in pcJun abundance with concurrent Rac1 inhibition (Figures 3A and 3D). To parse this potential *in vitro* confounder, HBC-specific *Rac1* cKO *in vivo* demonstrated that activated HBCs at 24 hpi indeed express attenuated nuclear pcJun (Figures 5E–5J and 5L). This biological recapitulation is unsurprising as *in vitro* HBCs treated with 50 nM PMA for 12 h bear a striking transcriptomic resemblance to *in vivo* HBCs activated by OE injury.[12] Firstly,

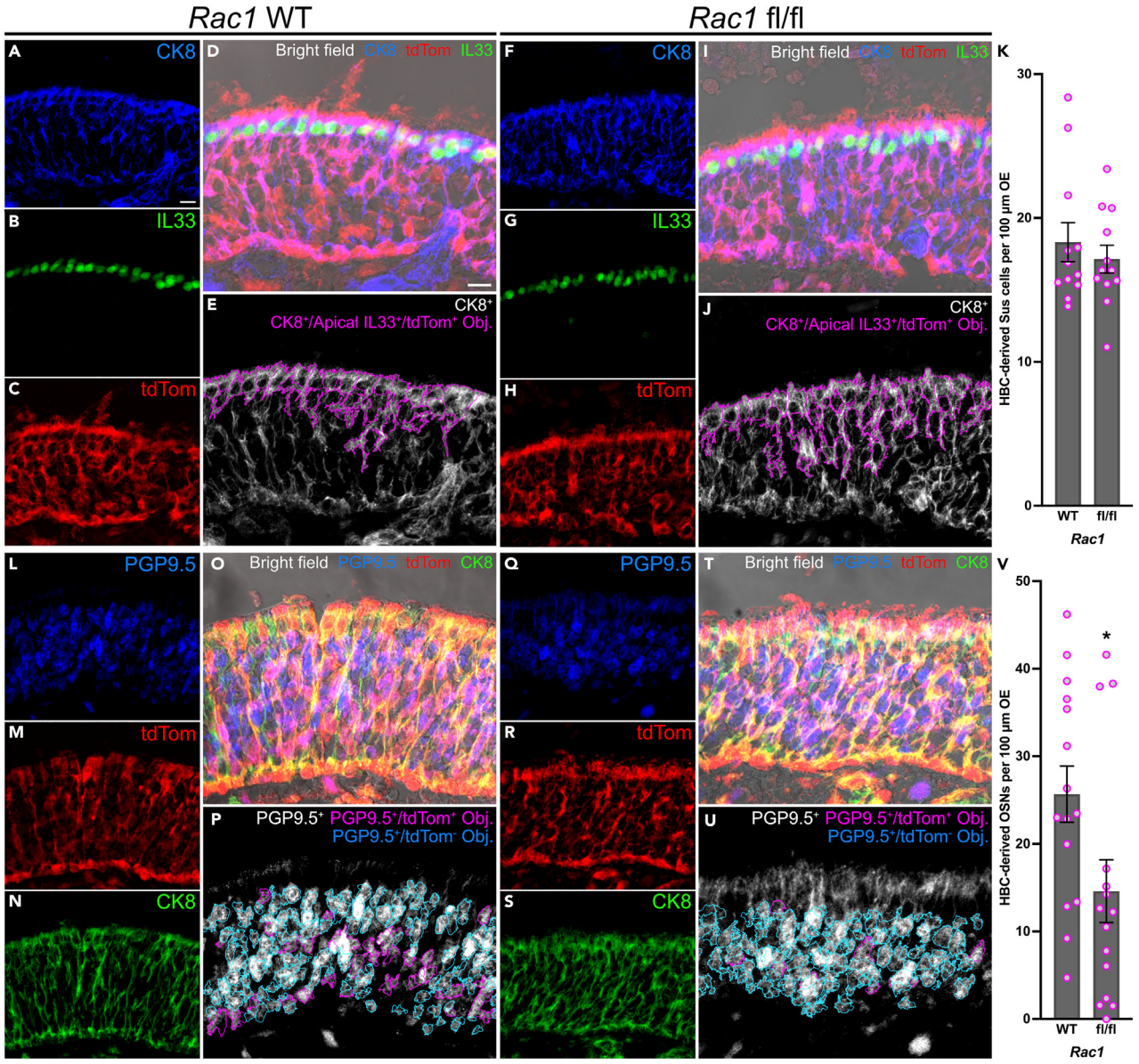

Figure 6. *In vivo* HBC neurogenesis following OE injury is diminished by HBC-specific *Rac1* cKO

(A–J) Representative immunofluorescence images demonstrating that HBC differentiation into CK8$^+$/apical IL33$^+$/tdTom$^+$ Sus cells (magenta in D and I; magenta outlines in E and J) is not significantly altered at 28 dpi by HBC-specific *Rac1* cKO (F–J) relative to *Rac1* WT (A–E).

(K) Quantification of HBC-derived Sus cells found in regenerated OE at 28 dpi; each circle denotes an analyzed region as represented in (E) and (J) (n = 12 regions across 3 mice).

(L–U) Representative immunofluorescence images demonstrating that fewer PGP9.5$^+$/tdTom$^+$ OSNs (magenta in O and T; magenta outlines in P and U) arise from HBCs at 28 dpi following HBC-specific *Rac1* cKO (Q–U) relative to *Rac1* WT (L–P).

(V) Quantification of HBC-derived OSNs found in regenerated OE at 28 dpi; each circle denotes an analyzed region as represented in (P) and (U) (n = 15 regions across 3 mice). Error bars indicate mean ± SEM, Mann-Whitney test, *p < 0.05 (K, V). Scale bar equals 10 µm (A, D).

decomposition of bulk RNA sequencing from PMA-treated *in vitro* HBCs demonstrates that the proportion of *in vitro* HBCs activated by 50 nM PMA proceeds in a temporally accurate manner when referenced against single-cell transcriptomes of *in vivo* HBCs from injured OE. Furthermore, when benchmarked against single-cell RNA sequencing of activated *in vivo* HBCs through 24 hpi,[10] PMA-treated *in vitro* HBCs and their *in vivo* counterparts share core transcriptional elements as evidenced by significant overlap in the top 100 differentially expressed genes. These sets notably include enhancement of multiple wound response genes, upregulation of *Hopx*, and downregulation of *p63*,[12] the latter two of which were again demonstrated (Figures 3A, 3B, 4A, 4B, and 4E). In addition to these extensive molecular data, PMA is known to activate

Itgb1-mediated signaling pathways[66] that can promote appropriate proliferation of mammary epithelial stem cells during mammary morphogenesis.[67] This understanding in tandem with the *in vivo* data presented here following injury demonstrating that HBCs mobilize molecular machinery integral to Itgb1-mediated signaling suggests that further mechanistic interrogation of these pathways will bear fruit.

PMA treatment of HBCs, however, did not recapitulate the increase in Ki67 seen during *in vivo* HBC activation.[7] Therefore, the decrease in Ki67 following PMA-induced HBC activation *in vitro* highlights the influence that *in situ* environmental cues may have on HBCs following OE injury. Given that skin wounding can prompt increased fibronectin deposition[68] and skeletal muscle damage is followed by changes in laminin expression,[69] the extracellular matrix (ECM) harbors promising candidate cues that are imperfectly recapitulated in the current culture model. Indeed, hematopoietic stem cell proliferation within bone marrow is dependent on interaction with tenascin-C,[70] while collagen VI in skeletal muscle acts as an instructive cue for satellite cells to proliferate.[71] In addition to positively regulating proliferation, chondroitin sulfate proteoglycans specify embryonic neural stem cell differentiation toward neuronal rather than glial fates.[72] Moreover, stem cell function dependent on ECM interactions can be mediated by Itgb1.[73,74] Therefore, our demonstration that *in vivo* HBCs spatiotemporally synchronize components of a signaling axis known to occur following Itgb1-ECM interactions[75,76] furthers the need to inquire about the spatial localization of and role that ECM proteins may play in regulating HBC biology following OE injury. Indeed, data demonstrating that HBC-specific *Rac1* cKO does not affect Itgb1 and Itgb4 expression at 24 hpi, including within the apical domain of HBCs (Figure S6), strengthen the case that Rac1 transduces signals initiated upstream by Itgb1 and/or Itgb4 interactions with currently unknown ECM components.

Limitations of the study

While the HBC cultures provided useful insights to motivate specific *in vivo* investigations, it is difficult to draw more definitive conclusions from these data given the use of small molecules had the relative biological simplicity inherent to *in vitro* systems. Due to technical limitations in our hands, we were unable to correlate *in vitro* Hopx expression to that *in vivo* before and after Rac1 perturbation. For this reason, we utilized a more indirect reference *in vivo*, namely HBC neuronal and Sus cell differentiation.

STAR★METHODS

Detailed methods are provided in the online version of this paper and include the following:

- KEY RESOURCES TABLE
- RESOURCE AVAILABILITY
  - Lead contact
  - Materials availability
  - Data and code availability
- EXPERIMENTAL MODEL AND STUDY PARTICIPANT DETAILS
  - Animals
- METHOD DETAILS
  - Tamoxifen induction of Cre-mediated recombination
  - Methimazole-induced OE injury
  - Tissue processing
  - Immunofluorescent labeling
  - Primary HBC culture
  - Western blot of primary HBCs
  - Immunocytochemistry
  - Imaging
  - Image analyses
  - Data presentation
- QUANTIFICATION AND STATISTICAL ANALYSIS

SUPPLEMENTAL INFORMATION

Supplemental information can be found online at https://doi.org/10.1016/j.isci.2024.109600.

ACKNOWLEDGMENTS

We would like to express immense gratitude to Po Kwok-Tse for her tremendous technical assistance. This work was supported by the NIH, USA: F30 DC018450 (J.D.L.) and R01 DC017869 (J.E.S.).

AUTHOR CONTRIBUTIONS

Conceptualization, J.D.L., C.M.B.-C., B.H.B., and J.E.S.; methodology, J.D.L.; formal analysis, J.D.L.; investigation, J.D.L., C.M.B-C., B.H.B., and C.A.H.; resources, J.E.S. and J.D.L.; writing – original draft, J.D.L.; writing – review and editing, J.D.L., C.M.B.-C., B.H.B., and J.E.S.; visualization, J.D.L.; funding acquisition, J.E.S. and J.D.L.

DECLARATION OF INTERESTS

J.E.S. is a co-founder of Rhino Therapeutics, Inc.

Received: May 22, 2022
Revised: December 21, 2023
Accepted: March 25, 2024
Published: March 27, 2024

REFERENCES

1. Leung, C.T., Coulombe, P.A., and Reed, R.R. (2007). Contribution of olfactory neural stem cells to tissue maintenance and regeneration. Nat. Neurosci. *10*, 720–726. https://doi.org/10.1038/nn1882.
2. Holbrook, E.H., Szumowski, K.E., and Schwob, J.E. (1995). An immunochemical, ultrastructural, and developmental characterization of the horizontal basal cells of rat olfactory epithelium. J. Comp. Neurol. *363*, 129–146. https://doi.org/10.1002/cne.903630111.
3. Herrick, D.B., Lin, B., Peterson, J., Schnittke, N., and Schwob, J.E. (2017). Notch1 maintains dormancy of olfactory horizontal basal cells, a reserve neural stem cell. Proc. Natl. Acad. Sci. USA *114*, E5589–E5598. https://doi.org/10.1073/pnas.1701333114.
4. Håglin, S., Berghard, A., and Bohm, S. (2020). Increased Retinoic Acid Catabolism in Olfactory Sensory Neurons Activates Dormant Tissue-Specific Stem Cells and Accelerates Age-Related Metaplasia. J. Neurosci. *40*, 4116–4129. https://doi.org/10.1523/JNEUROSCI.2468-19.2020.
5. Chen, M., Reed, R.R., and Lane, A.P. (2017). Acute inflammation regulates neuroregeneration through the NF-kappaB pathway in olfactory epithelium. Proc. Natl. Acad. Sci. USA *114*, 8089–8094. https://doi.org/10.1073/pnas.1620664114.
6. Joiner, A.M., Green, W.W., McIntyre, J.C., Allen, B.L., Schwob, J.E., and Martens, J.R. (2015). Primary Cilia on Horizontal Basal Cells Regulate Regeneration of the Olfactory Epithelium. J. Neurosci. *35*, 13761–13772. https://doi.org/10.1523/JNEUROSCI.1708-15.2015.
7. Fletcher, R.B., Prasol, M.S., Estrada, J., Baudhuin, A., Vranizan, K., Choi, Y.G., and Ngai, J. (2011). p63 regulates olfactory stem cell self-renewal and differentiation. Neuron *72*, 748–759. https://doi.org/10.1016/j.neuron.2011.09.009.
8. Schnittke, N., Herrick, D.B., Lin, B., Peterson, J., Coleman, J.H., Packard, A.I., Jang, W., and Schwob, J.E. (2015). Transcription factor p63 controls the reserve status but not the stemness of horizontal basal cells in the olfactory epithelium. Proc. Natl. Acad. Sci. USA *112*, E5068–E5077. https://doi.org/10.1073/pnas.1512272112.
9. Fletcher, R.B., Das, D., Gadye, L., Street, K.N., Baudhuin, A., Wagner, A., Cole, M.B., Flores, Q., Choi, Y.G., Yosef, N., et al. (2017). Deconstructing Olfactory Stem Cell Trajectories at Single-Cell Resolution. Cell Stem Cell *20*, 817–830.e8. https://doi.org/10.1016/j.stem.2017.04.003.
10. Gadye, L., Das, D., Sanchez, M.A., Street, K., Baudhuin, A., Wagner, A., Cole, M.B., Choi, Y.G., Yosef, N., Purdom, E., et al. (2017). Injury Activates Transient Olfactory Stem Cell States with Diverse Lineage Capacities. Cell Stem Cell *21*, 775–790.e9. https://doi.org/10.1016/j.stem.2017.10.014.
11. Peterson, J., Lin, B., Barrios-Camacho, C.M., Herrick, D.B., Holbrook, E.H., Jang, W., Coleman, J.H., and Schwob, J.E. (2019). Activating a Reserve Neural Stem Cell Population In Vitro Enables Engraftment and Multipotency after Transplantation. Stem Cell Rep. *12*, 680–695. https://doi.org/10.1016/j.stemcr.2019.02.014.
12. Barrios-Camacho, C.M., Zunitch, M.J., Louie, J.D., Jang, W., and Schwob, J.E. (2023). An in vitro model of acute horizontal basal cell activation reveals dynamic gene regulatory networks underlying the acute activation phase. Preprint at bioRxiv *2*. https://doi.org/10.1101/2023.12.14.568855.
13. Genter, M.B., Deamer, N.J., Blake, B.L., Wesley, D.S., and Levi, P.E. (1995). Olfactory toxicity of methimazole: dose-response and structure-activity studies and characterization of flavin-containing monooxygenase activity in the Long-Evans rat olfactory mucosa. Toxicol. Pathol. *23*, 477–486. https://doi.org/10.1177/019262339502300404.
14. Carroll, D.K., Carroll, J.S., Leong, C.O., Cheng, F., Brown, M., Mills, A.A., Brugge, J.S., and Ellisen, L.W. (2006). p63 regulates an adhesion programme and cell survival in epithelial cells. Nat. Cell Biol. *8*, 551–561. https://doi.org/10.1038/ncb1420.
15. Casaletto, J.B., Saotome, I., Curto, M., and McClatchey, A.I. (2011). Ezrin-mediated apical integrity is required for intestinal homeostasis. Proc. Natl. Acad. Sci. USA *108*, 11924–11929. https://doi.org/10.1073/pnas.1103418108.
16. Berrier, A.L., Martinez, R., Bokoch, G.M., and LaFlamme, S.E. (2002). The integrin beta tail is required and sufficient to regulate adhesion signaling to Rac1. J. Cell Sci. *115*, 4285–4291. https://doi.org/10.1242/jcs.00109.
17. Cruz-Monserrate, Z., and O'Connor, K.L. (2008). Integrin alpha 6 beta 4 promotes migration, invasion through Tiam1 upregulation, and subsequent Rac activation. Neoplasia *10*, 408–417. https://doi.org/10.1593/neo.07868.
18. Russell, A.J., Fincher, E.F., Millman, L., Smith, R., Vela, V., Waterman, E.A., Dey, C.N., Guide, S., Weaver, V.M., and Marinkovich, M.P. (2003). Alpha 6 beta 4 integrin regulates keratinocyte chemotaxis through differential GTPase activation and antagonism of alpha 3 beta 1 integrin. J. Cell Sci. *116*, 3543–3556. https://doi.org/10.1242/jcs.00663.
19. Didsbury, J., Weber, R.F., Bokoch, G.M., Evans, T., and Snyderman, R. (1989). rac, a novel ras-related family of proteins that are botulinum toxin substrates. J. Biol. Chem. *264*, 16378–16382.
20. ten Klooster, J.P., and Hordijk, P.L. (2007). Targeting and localized signalling by small GTPases. Biol. Cell *99*, 1–12. https://doi.org/10.1042/BC20060071.
21. Benitah, S.A., Frye, M., Glogauer, M., and Watt, F.M. (2005). Stem cell depletion through epidermal deletion of Rac1. Science *309*, 933–935. https://doi.org/10.1126/science.1113579.
22. Castilho, R.M., Squarize, C.H., Leelahavanichkul, K., Zheng, Y., Bugge, T., and Gutkind, J.S. (2010). Rac1 is required for epithelial stem cell function during dermal and oral mucosal wound healing but not for tissue homeostasis in mice. PLoS One *5*, e10503. https://doi.org/10.1371/journal.pone.0010503.
23. Myant, K.B., Scopelliti, A., Haque, S., Vidal, M., Sansom, O.J., and Cordero, J.B. (2013). Rac1 drives intestinal stem cell proliferation and regeneration. Cell Cycle *12*, 2973–2977. https://doi.org/10.4161/cc.26031.
24. Olabi, S., Ucar, A., Brennan, K., and Streuli, C.H. (2018). Integrin-Rac signalling for mammary epithelial stem cell self-renewal. Breast Cancer Res. *20*, 128. https://doi.org/10.1186/s13058-018-1048-1.
25. Deramaudt, T.B., Dujardin, D., Hamadi, A., Noulet, F., Kolli, K., De Mey, J., Takeda, K., and Rondé, P. (2011). FAK phosphorylation at Tyr-925 regulates cross-talk between focal adhesion turnover and cell protrusion. Mol. Biol. Cell *22*, 964–975. https://doi.org/10.1091/mbc.E10-08-0725.
26. Bohmann, D., Bos, T.J., Admon, A., Nishimura, T., Vogt, P.K., and Tjian, R. (1987). Human proto-oncogene c-jun encodes a DNA binding protein with structural and functional properties of transcription factor AP-1. Science *238*, 1386–1392. https://doi.org/10.1126/science.2825349.
27. Rauscher, F.J., 3rd, Voulalas, P.J., Franza, B.R., Jr., and Curran, T. (1988). Fos and Jun bind cooperatively to the AP-1 site: reconstitution in vitro. Genes Dev. *2*, 1687–1699. https://doi.org/10.1101/gad.2.12b.1687.
28. Shaulian, E., and Karin, M. (2001). AP-1 in cell proliferation and survival. Oncogene *20*, 2390–2400. https://doi.org/10.1038/sj.onc.1204383.
29. Han, S.I., Oh, S.Y., Woo, S.H., Kim, K.H., Kim, J.H., Kim, H.D., and Kang, H.S. (2001). Implication of a small GTPase Rac1 in the activation of c-Jun N-terminal kinase and heat shock factor in response to heat shock. J. Biol. Chem. *276*, 1889–1895. https://doi.org/10.1074/jbc.M006042200.
30. Louie, J.D., Bromberg, B.H., Zunitch, M.J., and Schwob, J.E. (2023). Horizontal basal cells self-govern their neurogenic potential during injury-induced regeneration of the olfactory epithelium. Development *150*, dev201552. https://doi.org/10.1242/dev.201552.
31. Seo, H.H., Lee, C.Y., Lee, J., Lim, S., Choi, E., Park, J.C., Lee, S., and Hwang, K.C. (2016). The role of nuclear factor of activated T cells during phorbol myristate acetate-induced cardiac differentiation of mesenchymal stem

cells. Stem Cell Res. Ther. *7*, 90. https://doi.org/10.1186/s13287-016-0348-6.

32. Song, J.K., Lee, C.H., Hwang, S.M., Joo, B.S., Lee, S.Y., and Jung, J.S. (2014). Effect of phorbol 12-myristate 13-acetate on the differentiation of adipose-derived stromal cells from different subcutaneous adipose tissue depots. Korean J. Physiol. Pharmacol. *18*, 289–296. https://doi.org/10.4196/kjpp.2014.18.4.289.
33. Shutes, A., Onesto, C., Picard, V., Leblond, B., Schweighoffer, F., and Der, C.J. (2007). Specificity and mechanism of action of EHT 1864, a novel small molecule inhibitor of Rac family small GTPases. J. Biol. Chem. *282*, 35666–35678. https://doi.org/10.1074/jbc.M703571200.
34. Teramoto, H., Coso, O.A., Miyata, H., Igishi, T., Miki, T., and Gutkind, J.S. (1996). Signaling from the small GTP-binding proteins Rac1 and Cdc42 to the c-Jun N-terminal kinase/stress-activated protein kinase pathway. A role for mixed lineage kinase 3/protein-tyrosine kinase 1, a novel member of the mixed lineage kinase family. J. Biol. Chem. *271*, 27225–27228. https://doi.org/10.1074/jbc.271.44.27225.
35. Smeal, T., Binetruy, B., Mercola, D., Grover-Bardwick, A., Heidecker, G., Rapp, U.R., and Karin, M. (1992). Oncoprotein-mediated signalling cascade stimulates c-Jun activity by phosphorylation of serines 63 and 73. Mol. Cell Biol. *12*, 3507–3513. https://doi.org/10.1128/mcb.12.8.3507-3513.1992.
36. Mohri, T., Adachi, Y., Ikehara, S., Hioki, K., Tokunaga, R., and Taketani, S. (1999). Activated Rac1 selectively up-regulates the expression of integrin alpha6beta4 and induces cell adhesion and membrane ruffles of nonadherent colon cancer Colo201 cells. Exp. Cell Res. *253*, 533–540. https://doi.org/10.1006/excr.1999.4720.
37. Kiosses, W.B., Shattil, S.J., Pampori, N., and Schwartz, M.A. (2001). Rac recruits high-affinity integrin alphavbeta3 to lamellipodia in endothelial cell migration. Nat. Cell Biol. *3*, 316–320. https://doi.org/10.1038/35060120.
38. Maurya, D.K., Henriques, T., Marini, M., Pedemonte, N., Galietta, L.J.V., Rock, J.R., Harfe, B.D., and Menini, A. (2015). Development of the Olfactory Epithelium and Nasal Glands in TMEM16A-/- and TMEM16A+/+ Mice. PLoS One *10*, e0129171. https://doi.org/10.1371/journal.pone.0129171.
39. Zunitch, M.J., Fisch, A.S., Lin, B., Barrios-Camacho, C.M., Faquin, W.C., Tachie-Baffour, Y., Louie, J.D., Jang, W., Curry, W.T., Gray, S.T., et al. (2023). Molecular Evidence for Olfactory Neuroblastoma as a Tumor of Malignant Globose Basal Cells. Mod. Pathol. *36*, 100122. https://doi.org/10.1016/j.modpat.2023.100122.
40. Nishijima, H., Zunitch, M.J., Yoshida, M., Kondo, K., Yamasoba, T., Schwob, J.E., and Holbrook, E.H. (2022). Rapid fluorescent vital imaging of olfactory epithelium. iScience *25*, 104222. https://doi.org/10.1016/j.isci.2022.104222.
41. Gavid, M., Coulomb, L., Thomas, J., Aouimeur, I., Verhoeven, P., Mentek, M., Dumollard, J.M., Forest, F., Prades, J.M., Thuret, G., et al. (2023). Technique of flat-mount immunostaining for mapping the olfactory epithelium and counting the olfactory sensory neurons. PLoS One *18*, e0280497. https://doi.org/10.1371/journal.pone.0280497.
42. Holbrook, E.H., Wu, E., Curry, W.T., Lin, D.T., and Schwob, J.E. (2011). Immunohistochemical characterization of human olfactory tissue. Laryngoscope *121*, 1687–1701. https://doi.org/10.1002/lary.21856.
43. Doty, R.L., Shaman, P., Applebaum, S.L., Giberson, R., Siksorski, L., and Rosenberg, L. (1984). Smell identification ability: changes with age. Science *226*, 1441–1443. https://doi.org/10.1126/science.6505700.
44. Doty, R.L. (2005). Clinical studies of olfaction. Chem. Senses *30* (*Suppl 1*), i207–i209. https://doi.org/10.1093/chemse/bjh187.
45. Fitzek, M., Patel, P.K., Solomon, P.D., Lin, B., Hummel, T., Schwob, J.E., and Holbrook, E.H. (2022). Integrated age-related immunohistological changes occur in human olfactory epithelium and olfactory bulb. J. Comp. Neurol. *530*, 2154–2175. https://doi.org/10.1002/cne.25325.
46. Child, K.M., Herrick, D.B., Schwob, J.E., Holbrook, E.H., and Jang, W. (2018). The Neuroregenerative Capacity of Olfactory Stem Cells Is Not Limitless: Implications for Aging. J. Neurosci. *38*, 6806–6824. https://doi.org/10.1523/JNEUROSCI.3261-17.2018.
47. Schwob, J.E., Jang, W., Holbrook, E.H., Lin, B., Herrick, D.B., Peterson, J.N., and Hewitt Coleman, J. (2017). Stem and progenitor cells of the mammalian olfactory epithelium: Taking poietic license. J. Comp. Neurol. *525*, 1034–1054. https://doi.org/10.1002/cne.24105.
48. Hildebrand, M.S., Dahl, H.H.M., Hardman, J., Coleman, B., Shepherd, R.K., and de Silva, M.G. (2005). Survival of partially differentiated mouse embryonic stem cells in the scala media of the guinea pig cochlea. J. Assoc. Res. Otolaryngol. *6*, 341–354. https://doi.org/10.1007/s10162-005-0012-9.
49. Hampsch, R.A., Shee, K., Bates, D., Lewis, L.D., Désiré, L., Leblond, B., Demidenko, E., Stefan, K., Huang, Y.H., and Miller, T.W. (2017). Therapeutic sensitivity to Rac GTPase inhibition requires consequential suppression of mTORC1, AKT, and MEK signaling in breast cancer. Oncotarget *8*, 21806–21817. https://doi.org/10.18632/oncotarget.15586.
50. Désiré, L., Bourdin, J., Loiseau, N., Peillon, H., Picard, V., De Oliveira, C., Bachelot, F., Leblond, B., Taverne, T., Beausoleil, E., et al. (2005). RAC1 inhibition targets amyloid precursor protein processing by gamma-secretase and decreases Abeta production in vitro and in vivo. J. Biol. Chem. *280*, 37516–37525. https://doi.org/10.1074/jbc.M507913200.
51. Ramos, D.F.V., Mancuso, R.I., Contieri, B., Duarte, A., Paiva, L., de Melo Carrilho, J., Saad, S.T.O., and Lazarini, M. (2022). Rac GTPases in acute myeloid leukemia cells: Expression profile and biological effects of pharmacological inhibition. Toxicol. Appl. Pharmacol. *442*, 115990. https://doi.org/10.1016/j.taap.2022.115990.
52. Wang, R., Yu, Q., Wang, X., Li, B., Ciotkowska, A., Rutz, B., Wang, Y., Stief, C.G., and Hennenberg, M. (2020). Rac1 silencing, NSC23766 and EHT1864 reduce growth and actin organization of bladder smooth muscle cells. Life Sci. *261*, 118468. https://doi.org/10.1016/j.lfs.2020.118468.
53. Dütting, S., Heidenreich, J., Cherpokova, D., Amin, E., Zhang, S.C., Ahmadian, M.R., Brakebusch, C., and Nieswandt, B. (2015). Critical off-target effects of the widely used Rac1 inhibitors NSC23766 and EHT1864 in mouse platelets. J. Thromb. Haemost. *13*, 827–838. https://doi.org/10.1111/jth.12861.
54. Corbetta, S., Gualdoni, S., Ciceri, G., Monari, M., Zuccaro, E., Tybulewicz, V.L.J., and de Curtis, I. (2009). Essential role of Rac1 and Rac3 GTPases in neuronal development. FASEB J. *23*, 1347–1357. https://doi.org/10.1096/fj.08-121574.
55. Haditsch, U., Anderson, M.P., Freewoman, J., Cord, B., Babu, H., Brakebusch, C., and Palmer, T.D. (2013). Neuronal Rac1 is required for learning-evoked neurogenesis. J. Neurosci. *33*, 12229–12241. https://doi.org/10.1523/JNEUROSCI.2939-12.2013.
56. Vadodaria, K.C., Brakebusch, C., Suter, U., and Jessberger, S. (2013). Stage-specific functions of the small Rho GTPases Cdc42 and Rac1 for adult hippocampal neurogenesis. J. Neurosci. *33*, 1179–1189. https://doi.org/10.1523/JNEUROSCI.2103-12.2013.
57. Liang, X., Draghi, N.A., and Resh, M.D. (2004). Signaling from integrins to Fyn to Rho family GTPases regulates morphologic differentiation of oligodendrocytes. J. Neurosci. *24*, 7140–7149. https://doi.org/10.1523/JNEUROSCI.5319-03.2004.
58. Breipohl, W., Laugwitz, H.J., and Bornfeld, N. (1974). Topological relations between the dendrites of olfactory sensory cells and sustentacular cells in different vertebrates. An ultrastructural study. J. Anat. *117*, 89–94.
59. Dahl, A.R., Hadley, W.M., Hahn, F.F., Benson, J.M., and McClellan, R.O. (1982). Cytochrome P-450-dependent monooxygenases in olfactory epithelium of dogs: possible role in tumorigenicity. Science *216*, 57–59. https://doi.org/10.1126/science.7063870.
60. Rafols, J.A., and Getchell, T.V. (1983). Morphological relations between the receptor neurons, sustentacular cells and Schwann cells in the olfactory mucosa of the salamander. Anat. Rec. *206*, 87–101. https://doi.org/10.1002/ar.1092060111.
61. Suzuki, Y., Takeda, M., and Farbman, A.I. (1996). Supporting cells as phagocytes in the olfactory epithelium after bulbectomy. J. Comp. Neurol. *376*, 509–517. https://doi.org/10.1002/(SICI)1096-9861(19961223)376:4<509::AID-CNE1>3.0.CO;2-5.
62. Mertens, A.E.E., Rygiel, T.P., Olivo, C., van der Kammen, R., and Collard, J.G. (2005). The Rac activator Tiam1 controls tight junction biogenesis in keratinocytes through binding to and activation of the Par polarity complex. J. Cell Biol. *170*, 1029–1037. https://doi.org/10.1083/jcb.200502129.
63. Guillemot, L., Guerrera, D., Spadaro, D., Tapia, R., Jond, L., and Citi, S. (2014). MgcRacGAP interacts with cingulin and paracingulin to regulate Rac1 activation and development of the tight junction barrier during epithelial junction assembly. Mol. Biol. Cell *25*, 1995–2005. https://doi.org/10.1091/mbc.E13-11-0680.
64. Castagna, M., Takai, Y., Kaibuchi, K., Sano, K., Kikkawa, U., and Nishizuka, Y. (1982). Direct activation of calcium-activated, phospholipid-dependent protein kinase by tumor-promoting phorbol esters. J. Biol. Chem. *257*, 7847–7851.
65. Adler, V., Franklin, C.C., and Kraft, A.S. (1992). Phorbol esters stimulate the phosphorylation of c-Jun but not v-Jun: regulation by the N-terminal delta domain. Proc. Natl. Acad. Sci. USA *89*, 5341–5345. https://doi.org/10.1073/pnas.89.12.5341.
66. Hellweg, C.E., Arenz, A., Bogner, S., Schmitz, C., and Baumstark-Khan, C. (2006). Activation

of nuclear factor kappa B by different agents: influence of culture conditions in a cell-based assay. Ann. N. Y. Acad. Sci. *1091*, 191–204. https://doi.org/10.1196/annals.1378.066.

67. Taddei, I., Deugnier, M.A., Faraldo, M.M., Petit, V., Bouvard, D., Medina, D., Fässler, R., Thiery, J.P., and Glukhova, M.A. (2008). Beta1 integrin deletion from the basal compartment of the mammary epithelium affects stem cells. Nat. Cell Biol. *10*, 716–722. https://doi.org/10.1038/ncb1734.
68. To, W.S., and Midwood, K.S. (2011). Plasma and cellular fibronectin: distinct and independent functions during tissue repair. Fibrogenesis Tissue Repair *4*, 21. https://doi.org/10.1186/1755-1536-4-21.
69. Rayagiri, S.S., Ranaldi, D., Raven, A., Mohamad Azhar, N.I.F., Lefebvre, O., Zammit, P.S., and Borycki, A.G. (2018). Basal lamina remodeling at the skeletal muscle stem cell niche mediates stem cell self-renewal. Nat. Commun. *9*, 1075. https://doi.org/10.1038/s41467-018-03425-3.
70. Nakamura-Ishizu, A., Okuno, Y., Omatsu, Y., Okabe, K., Morimoto, J., Uede, T., Nagasawa, T., Suda, T., and Kubota, Y. (2012). Extracellular matrix protein tenascin-C is required in the bone marrow microenvironment primed for hematopoietic regeneration. Blood *119*, 5429–5437. https://doi.org/10.1182/blood-2011-11-393645.
71. Urciuolo, A., Quarta, M., Morbidoni, V., Gattazzo, F., Molon, S., Grumati, P., Montemurro, F., Tedesco, F.S., Blaauw, B., Cossu, G., et al. (2013). Collagen VI regulates satellite cell self-renewal and muscle regeneration. Nat. Commun. *4*, 1964. https://doi.org/10.1038/ncomms2964.
72. Sirko, S., von Holst, A., Wizenmann, A., Götz, M., and Faissner, A. (2007). Chondroitin sulfate glycosaminoglycans control proliferation, radial glia cell differentiation and neurogenesis in neural stem/progenitor cells. Development *134*, 2727–2738. https://doi.org/10.1242/dev.02871.
73. Brizzi, M.F., Tarone, G., and Defilippi, P. (2012). Extracellular matrix, integrins, and growth factors as tailors of the stem cell niche. Curr. Opin. Cell Biol. *24*, 645–651. https://doi.org/10.1016/j.ceb.2012.07.001.
74. Shen, Q., Wang, Y., Kokovay, E., Lin, G., Chuang, S.M., Goderie, S.K., Roysam, B., and Temple, S. (2008). Adult SVZ stem cells lie in a vascular niche: a quantitative analysis of niche cell-cell interactions. Cell Stem Cell *3*, 289–300. https://doi.org/10.1016/j.stem.2008.07.026.
75. Lawson, C.D., and Burridge, K. (2014). The on-off relationship of Rho and Rac during integrin-mediated adhesion and cell migration. Small GTPases *5*, e27958. https://doi.org/10.4161/sgtp.27958.
76. Yu, W., Datta, A., Leroy, P., O'Brien, L.E., Mak, G., Jou, T.S., Matlin, K.S., Mostov, K.E., and Zegers, M.M.P. (2005). Beta1-integrin orients epithelial polarity via Rac1 and laminin. Mol. Biol. Cell *16*, 433–445. https://doi.org/10.1091/mbc.e04-05-0435.
77. Indra, A.K., Warot, X., Brocard, J., Bornert, J.M., Xiao, J.H., Chambon, P., and Metzger, D. (1999). Temporally-controlled site-specific mutagenesis in the basal layer of the epidermis: comparison of the recombinase activity of the tamoxifen-inducible Cre-ER(T) and Cre-ER(T2) recombinases. Nucleic Acids Res. *27*, 4324–4327. https://doi.org/10.1093/nar/27.22.4324.
78. Xiong, D., Hu, W., Han, X., and Cai, Y. (2023). Rhein Inhibited Ferroptosis and EMT to Attenuate Diabetic Nephropathy by Regulating the Rac1/NOX1/beta-Catenin Axis. Front. Biosci. *28*, 100. https://doi.org/10.31083/j.fbl2805100.
79. Su, Y., Huang, H., Luo, T., Zheng, Y., Fan, J., Ren, H., Tang, M., Niu, Z., Wang, C., Wang, Y., et al. (2022). Cell-in-cell structure mediates in-cell killing suppressed by CD44. Cell Discov. *8*, 35. https://doi.org/10.1038/s41421-022-00387-1.
80. Lamprecht, M.R., Sabatini, D.M., and Carpenter, A.E. (2007). CellProfiler: free, versatile software for automated biological image analysis. Biotechniques *42*, 71–75. https://doi.org/10.2144/000112257.

STAR★METHODS

KEY RESOURCES TABLE

REAGENT or RESOURCE	SOURCE	IDENTIFIER
Antibodies		
Mouse α-p63	ATCC	Clone 4A4
Mouse α-Ezrin	Developmental Studies Hybridoma Bank	CPTC-Ezrin-1
Rabbit α-Laminin	Novus Biologicals	NB300-144
Goat α-Itgb1	R&D Systems	AF2405
Rat α-Itgb4	R&D Systems	MAB4054
Chicken α-CK5	BioLegend	Clone Poly9059
Rabbit α-Rac1	Proteintech	24072-1-AP
Rabbit α-pFAKY925	Cell Signaling Technology	3284
Rabbit α-pcJun	Cell Signaling Technology	3270
Rabbit α-PGP9.5	Proteintech	14730-1-AP
Rabbit α-ΔNp63	BioLegend	619002
Rabbit α-cJun	Cell Signaling Technology	9165
Rabbit α-JNK	Cell Signaling Technology	9252
Rabbit α-pJNK	Cell Signaling Technology	4668
Mouse α-Rac1	Proteintech	66122-1-Ig
Mouse α-GAPDH	Cell Signaling Technology	97166
Chemicals, peptides, and recombinant proteins		
Tamoxifen	Sigma-Aldrich	T5648
Corn oil	Spectrum Chemical	CO136
4-hydroxytamoxifen	Hello Bio	HB6040
Sunflower oil	Sigma-Aldrich	S5007
Castor oil	Sigma-Aldrich	259853
Methimazole	Sigma-Aldrich	M8506
EHT1864	SellekChem	S7482
Phorbol 12-myristate 13-acetate	SellekChem	S7791
Critical commercial assays		
RIPA Lysis and Extraction Buffer	Thermo Scientific	89901
Halt Protease and Phosphatase Inhibitor	Thermo Scientific	78442
Pierce BCA Protein Assay Kit	Thermo Scientific	23227
4X Bolt LDS Sample Buffer	Invitrogen	B0007
10X Bolt Sample Reducing Agent	Invitrogen	B0009
Bolt 4-12% Bis-Tris Plus Mini Protein Gel	Invitrogen	NW04120BOX
Broad Range Prestained Protein Marker	Proteintech	PL00002
20X Bolt MES SDS Running Buffer	Invitrogen	B0002
PVDF/Filter Paper Sandwich (0.2 μm)	Invitrogen	LC2002
20X Bolt Transfer Buffer	Invitrogen	BT00061
SuperSignal West Pico PLUS Chemiluminescent Substrate	Thermo Scientific	34577
Experimental models: Cell lines		
Rat: primary HBCs	Taconic Biosciences	SD-M

(*Continued on next page*)

Continued

REAGENT or RESOURCE	SOURCE	IDENTIFIER
Experimental models: Organisms/strains		
Mouse: C57BL/6J; 129S1/SvlmJ F2 (wild-type)	This paper	N/A
Mouse: *K5CreER^{T2}*	Indra et al., 1999	MGI:2177427
Mouse: *Rosa26R(tdTomato)*	The Jackson Laboratory	007909
Mouse: *Rac1^{tm1Djk}*/J	The Jackson Laboratory	005550
Software and algorithms		
ImageJ	National Institutes of Health	https://imagej.net/ij/index.html
CellProfiler	Lamprecht et al., 2007	https://cellprofiler.org/
Affinity Designer	Serif Europe Ltd.	https://affinity.serif.com/en-us/designer/
GraphPad Prism 10	GraphPad Software	https://www.graphpad.com/

RESOURCE AVAILABILITY

Lead contact

Further information and requests for resources and reagents should be directed to and will be fulfilled by the lead contact, James E. Schwob (jim.schwob@tufts.edu).

Materials availability

This study did not generate new unique reagents.

Data and code availability

- All data reported in this paper will be shared by the lead contact upon request.
- This paper does not report original code.
- Any additional information required to reanalyze the data reported in this paper is available from the lead contact upon request.

EXPERIMENTAL MODEL AND STUDY PARTICIPANT DETAILS

Animals

All animals were maintained on *ad libitum* chow and water in a heat and humidity controlled, AALAC-accredited vivarium. All protocols for the use of vertebrate animal were approved by the Committee for the Humane Use of Animals at Tufts University School of Medicine. *In vitro* primary HBCs were harvested from male and female Sprague-Dawley rats (Taconic Biosciences, Cat. SD-M). WT mice were F2 generation mice from an initial cross of C57BL/6J (Jax Stock #000664) and 129S1/SvlmJ (Jax Stock #002448) mice performed in-house. *K5CreER^{T2}* mice, which enable HBC-specific inducible recombination, were generously provided by Dr. Pierre Chambon.[77] *Rosa26R(tdTomato)* (Jax Stock #007909) mice were obtained from Jackson Labs. *Rac1^{tm1Djk}*/J (Jax Stock #005550) mice were generously transferred from the Rejji Kuruvilla Lab, Johns Hopkins University. Bi-genic *K5CreER^{T2}*; *Rosa26R(tdTomato)* (KT) mice enabling HBC-specific inducible lineage tracing were generated in-house. Tri-genic *K5CreER^{T2}*; *Rac1$^{tm1Djk/\ tm1Djk}$* /J; *Rosa26R(tdTomato)* (*Rac1* fl/fl) mice enabling HBC-specific inducible *Rac1* KO and lineage tracing were generated in-house. *K5CreER^{T2}*; *Rac1$^{WT/\ WT}$* /J; *Rosa26R(tdTomato)* mice (*Rac1* WT) served as controls for genetic recombination experiments. All *in vivo* experiments used sex- and age-matched male and female mice that were 8-12 weeks old when initiated.

METHOD DETAILS

Tamoxifen induction of Cre-mediated recombination

Tamoxifen (Sigma-Aldrich, Cat. T5648) was dissolved in corn oil (Spectrum Chemical, Cat. CO136) at a stock concentration of 30 mg/mL. This tamoxifen stock was used to perform intra-peritoneal (IP) injections of KT mice at 150 mg/kg for two consecutive days prior to subsequent experimentation. 4-hydroxytamoxifen (Hello Bio, Cat. HB6040) was dissolved in 100% ethanol (Fisher Scientific, Cat. BP2818) at a stock concentration of 40 mg/mL. Prior to IP injection, this stock was emulsified in a mixture of 4 parts sunflower oil (Sigma-Aldrich, Cat. S5007) and 1 part castor oil (Sigma-Aldrich, Cat. 259853). *Rac1* WT and *Rac1* fl/fl mice each received 2.5mg 4-hydroxytamoxifen per day for five consecutive days prior to subsequent experimentation.

Methimazole-induced OE injury

Methimazole (MTZ) (Sigma-Aldrich, Cat. M8506) was dissolved in 1X PBS (Gibco, Cat. 10010-023) at a stock concentration of 5 mg/mL. WT mice received an IP injection at 10μL MTZ stock/g mouse. WT mice used for uninjured OE controls received an IP injection at 10 uL 1X

PBS vehicle/g mouse. KT mice received an IP injection at 10uL MTZ stock/g mouse 5 days after the initial tamoxifen injection. *Rac1* WT and *Rac1* fl/fl mice received an IP injection at 7.5μL MTZ stock/g mouse 21 days after the last 4-hydroxytamoxifen injection. This reduction in MTZ concentration was necessary as 10μL MTZ stock/g *Rac1* WT or fl/fl mouse resulted in OE over-lesioning as evidenced by the absence of $tdTom^+$ HBCs at 24 hpi.

Tissue processing

At indicated time points, mice were euthanized with an intra-muscular injection of ketamine (37.5mg/kg), xylazine (7.5mg/kg), and acepromazine (1.25mg/kg) triple cocktail. Following trans-cardial perfusion with 20mL PBS (Gibco Cat. 10010-023), mice were trans-cardially fixed with 40mL 1% PLP (1% paraformaldehyde, 0.1M monobasic and dibasic phosphates, 90mM lysine, and 0.1M meta-sodium periodate). After dissecting away the surrounding cranial structures, the isolated OE was post-fixed in 1% PLP under vacuum for 1.5hrs. Following post-fixation, the OE was briefly rinsed three times in 1X PBS to wash away residual fixative and then incubated in decalcification buffer (0.35M EDTA [Sigma-Aldrich, Cat. ED2SS] and 0.35M NaOH) overnight at 4°C. To cryopreserve the tissue, OE was equilibrated overnight in 30% sucrose (w/v in 1X PBS) at 4°C, embedded and frozen in OCT (Sakura, Cat. 4583), and then stored at −80°C until cryosectioning. A Leica cryostat was used to collect 10 μm coronal sections on positively-charged glass slides.

Immunofluorescent labeling

Specific antibodies and conditions to detect the various antigens can be found in Table S1. Of note, the Rac1 antibody utilized has been validated by knockdown experiments.[78,79] All primary antibodies were diluted in Normal Donkey Block (NDB) (10% normal donkey serum v/v, 5% non-fat powdered milk w/v, 4% bovine serum albumin [BSA] w/v, and 0.1% Triton X-100 v/v in 1X PBS). Species-specific fluorophore- and biotin-conjugated donkey secondary antibodies (Jackson ImmunoResearch) were diluted in NDB at 1:150 and 1:100, respectively. Streptavidin-conjugated horseradish peroxidase (SA-HRP) was diluted in TNB (0.5% blocking reagent w/v [Akoya Biosciences, Cat. FP1020], 0.15M NaCl, and 0.1M Tris-HCl pH 7.5) at 1:400. All washes performed on day 1 and day 2 were in 1X PBS and 3X PBS, respectively, with those following antibody incubation performed 3x5min. Slides were dried on a slide warmer at ~37°C for 45-60min. after application of rubber cement (Elmer's) to isolate each section. Following a 10-15min. wash to remove OCT, sections used to detect antigens requiring antigen retrieval were incubated in antigen retrieval buffer (0.1M sodium citrate, pH 6) and placed in a pre-heated commercial steamer for 10min. After slides were washed for 10min., sections were permeabilized with 90% MeOH for 5min. Sections designated to detect antigens requiring tyramide signal amplication (TSA) were incubated for 5min. in 3% H_2O_2 diluted in MeOH in lieu of 90% MeOH. Slides were then washed 3x5min., and blocked for 1 hr. at room temperature with NDB. Following overnight primary antibody incubation at 4°C, sections were incubated in secondary antibodies for 1 hr. at room temperature in the dark. If antigen detection required TSA, appropriate sections were blocked for 30min. in TNB prior to incubation in SA-HRP for 1 hr. at room temperature in the dark. TSA was achieved by incubating appropriate sections for 15min. in a solution consisting of 98% TSA Buffer (0.1M boric acid pH 8.5, 0.003% H_2O_2), 1% of 10% BSA w/v in 1X PBS, and 1% FITC-tyramide. Nuclei were counterstained with DAPI. Sections were coverslipped in NPG (0.5% N-propyl gallate in 90% glycerol) mounting media, sealed with nail polish, and slides were stored at 4°C in the dark until imaging.

Primary HBC culture

Isolation, maintenance, and passaging of primary HBCs have been previously described in detail.[11] PMA (Sellekchem, Cat. S7791) and EHT1864 (SellekChem, Cat. S7482) were dissolved in DMSO. For all experiments, HBCs were treated with 50 nM PMA and 50 μM EHT1864. DMSO concentration for all conditions was identical at all times. EHT1864 attenuates Rac1 activation in a dose-dependent manner and it was used at 50 μM as this concentration maximally inhibits Rac1.[33] Passage 10 HBCs were used for all experiments and treated with the appropriate compounds for 12 hrs. prior to immediate lysis for western blot or fixation for immunocytochemistry. If determined to undergo Rac1 inhibition, HBCs were pre-incubated in 50 μM EHT1864 for 1 hr. HBCs cultured for western blot analyses were grown on 6-well plates coated with poly-D-lysine/laminin (Corning, Cat. 354595). HBCs cultured for immunocytochemistry were grown on 8-well culture slides coated with poly-D-lysine/laminin (Corning, Cat. 354688).

Western blot of primary HBCs

Primary HBCs were lysed by applying 200μL Lysis Buffer (RIPA buffer [Thermo Scientific, Cat. 89901] supplemented with a protease and phosphatase inhibitor cocktail [Thermo Scientific, Cat. 78442]) per well and freezing the 6-well plate at -80°C overnight. All subsequent steps were performed on ice. Immediately after thawing, an additional 100μL Lysis Buffer was applied to each well and mechanical cell lysis was performed with a cell scraper. The entire volume of lysate from each well was transferred to a pre-chilled 2mL microcentrifuge tube, and debris pelleted via centrifugation at maximum rpm for 10min. at 4°C. Supernatant from each experimental condition was transferred to a new pre-chilled 2mL microcentrifuge tube and total protein abundance was determined by BCA protein assay per manufacturer's protocol (Thermo Scientific, Cat. 23227). Working protein stocks were prepared by diluting supernatant with 4X LDS Sample Buffer (Invitrogen, Cat. B0007), 10X Sample Reducing Agent (Invitrogen, Cat. B0009), and Lysis Buffer. These stocks were placed in a heating block set at 70°C for 10min and then stored at -80°C.

Protein from working stocks were loaded at ~5μg in 4-12% Bis-Tris gels (Invitrogen, Cat. NW04120BOX) and bracketed by a protein ladder standard (Proteintech, Cat. PL00002). Gels were run per manufacturer's protocol (Invitrogen, Cat. A25977) in MES SDS running buffer

(Invitrogen, Cat. B0002). Protein was transferred to a 0.2 μm PVDF membrane (Invitrogen, Cat. LC2002) at 20V per manufacturer's protocol (Invitrogen, Cat. BT00061).

Following protein transfer, membranes were rinsed in 1X TBST (Tris-buffered saline with 1% Tween 20) and blocked for 1 hr. at room temperature in Blocking Buffer (5% BSA w/v in 1X TBST). Primary antibodies against ΔNp63 (BioLegend, Cat. 619002; 1:500), cJun (Cell Signaling Technology, Cat. 9165; 1:1000), pcJun (Cell Signaling Technology, Cat. 3270; 1:1000), JNK (Cell Signaling Technology, Cat. 9252; 1:1000), pJNK (Cell Signaling Technology, Cat. 4668; 1:1000), Rac1 (Proteintech, Cat. 66122-1-Ig; 1:2000), and GAPDH (Cell Signaling Technology, Cat. 97166; 1:1000) were diluted in Blocking Buffer and incubated with membranes overnight at 4°C. The following day, membranes were washed 6x7min. in 1X TBST, incubated in the appropriate HRP-conjugated donkey secondary antibodies (Jackson ImmunoResearch) diluted 1:5000 in Blocking Buffer, and washed 6x5min in 1X TBST. Proteins were visualized in a gel dock system (Bio-Rad, Universal Hood II) after membranes were incubated in SuperSignal West Pico Plus Chemiluminescent substrate (Thermo Scientific, Cat. 34577). Bio-Rad Image Lab software was used to export TIFF files that were subsequently imported into ImageJ to perform densitometric analyses. Protein abundance was calculated by normalizing the densitometric value of the protein band to that of its paired GAPDH band. Given similar molecular weights between cJun, pcJun, JNK, pJNK, and GAPDH, membranes used to first detect either cJun, pcJun, JNK, or pJNK were dried overnight to deactivate HRP conjugated to donkey anti-rabbit antibodies. Following their reactivation in 100% methanol, membranes were then washed in 1X TBST and processed as described above following overnight primary antibody incubation to visualize GAPDH via HRP conjugated to donkey anti-mouse antibodies.

Immunocytochemistry

Primary HBCs were fixed with 10% buffered formalin (Fisher, Cat. SF100) for 15min. at room temperature, washed 3x5min in 1X PBS, then stored at 4°C in fresh 1X PBS until further processing. To note, all washes prior to primary antibody incubation and during day 2 were in 1X PBS and 3X PBS, respectively, with those following antibody incubation performed 3x5min. HBCs were subsequently permeabilized on ice with ice-cold 100% MeOH for 10min. and washed 3x5min. After 1 hr. of blocking in NDB at room temperature, HBCs were incubated overnight at 4°C in antibodies against Hopx (1:150; Proteintech, Cat. 11419-1-AP), Ki67 (1:75; BD Biosciences, Cat. 556003), and CK5 (1:400; BioLegend, Clone Poly9059) in NDB diluent. The next day, HBCs were incubated in the dark with species-specific fluorophore-conjugated donkey secondary antibodies (Jackson ImmunoResearch) at 1:250 in NDB diluent. Nuclei were counterstained with DAPI. Chamber walls of culture slides were removed per manufacturer's protocol. Slides were coverslipped with NPG mounting media, sealed with nail polish, and stored at 4°C in the dark until imaging.

Imaging

All sections and cells were imaged on a Zeiss LSM800 confocal microscope. Zeiss Zen 2.6 software was used to set imaging parameters to eliminate spectral overlap between channels, which included capturing fluorescence in multi-track mode, adjusting the variable secondary dichroics, and enabling appropriate emission filters. For proteins quantified by relative fluorescence intensity, all excitation and emission capture settings were identical between control and experimental conditions. Imaging OE included capturing multiple z-planes stepped at 2 μm intervals to sample from a minimum of ~5 cellular cross-sections. First and last z-planes were established when the maximum fluorescence intensity of the channel to be quantified fell within lowest quartile of a 16bit display range. Because primary HBCs can pile on top of each another in culture, imaging HBC islands *in vitro* involved capturing the z-plane in which $CK5^+$ HBCs appeared most confluent.

Image analyses

ImageJ was used to process all uncompressed, 16bit tiff files obtained from confocal imaging. Z-planes were sum projected to maximize bit depth of captured fluorescence. The ImageJ Rolling ball background subtraction function was applied to every channel. CellProfiler image analysis software[80] was used to quantify total fluorescence intensity. Images of channels in which captured fluorescence was intended to facilitate cellular domain demarcation rather than for intensity quantification (namely Laminin, Ezrin, and CK5) were converted to 16bit so that CellProfiler could process those images, identify relevant cellular landmarks, and quantify the area that those landmarks occupied if applicable. The basal domain of HBCs was determined within CellProfiler and defined as $Laminin^+$ objects that overlapped with $CK5^+$ objects. The apical domain of HBCs was similarly determined within CellProfiler and defined as $Ezrin^+$ objects that overlapped with $CK5^+$ objects without encroaching on areas occupied by $Laminin^+$ objects. The differing appearance of $CK5^+$/ $Ezrin^+$ objects between Figures 1 and 2 are a result of mutually exclusive tissue processing requirements of Itgb1, Itgb4, Rac1, pFAKY925, and pcJun prior to primary antibody incubation. Specifically, antigen retrieval was necessary to immunolabel Rac1, pFAKY925, and pcJun, and enabled Ezrin detection via donkey anti-mouse IgG conjugated fluorophores. However, antigen retrieval had to be avoided in order to retain Itgb1 and Itgb4 antigenicity, which also then necessitated Ezrin detection via streptavidin-conjugated fluorophores. Moreover, antigen retrieval significantly compromised Laminin antigenicity, and as such, limited the ability to objectively demarcate HBC basal domains. Consequently, some $CK5^+$/ $Ezrin^+$ objects in Figure 2 appear sub-apical as images were sum projected for reasons stated above. For experiments quantifying relative fluorescence, the average fluorescence density of the control condition was used as the denominator to calculate normalized fluorescence densities. For analyses at 28 dpi, images acquired from the tdTom channel were used to morphologically identify and measure the length of the basal lamina using the freehand tool within ImageJ. To negate the potential bias associated with manual counting, CellProfiler was utilized to identify individual OSN objects via segmentation by Otsu thresholding of PGP9.5 fluorescence that co-localized with $DAPI^+$ nuclei (channel not shown

for illustrative clarity). These PGP9.5^{+} objects were counted as tdTom^{+} if at least 25% of their area co-localized with tdTom^{+}/CK8^{-} fluorescence as determined by CellProfiler.

Data presentation

Only brightness and contrast were adjusted for each representative image within ImageJ or Affinity Designer, and these parameters were applied globally to the image. Graphs were generated using GraphPad Prism Version 10. All figures were constructed in Affinity Designer.

QUANTIFICATION AND STATISTICAL ANALYSIS

All statistical analyses were performed with GraphPad Prism Version 10. For single mean comparisons, data sets demonstrating normal and non-normal distributions were compared with unpaired t-test and Mann-Whitney test, respectively. For multiple mean comparisons, data sets demonstrating normal and non-normal distributions were compared with one-way ANOVA with post-hoc Tukey's multiple comparisons test and Kruskal-Wallis test with post-hoc Dunn's multiple comparisons test, respectively. A p-value < 0.05 was considered statistically significant (*<0.05, **p<0.01, ***p<0.001, ****p<0.0001). Error bars indicate mean $\pm$ SEM.